Influence of the cobalt particle size in the CO hydrogenation reaction studied by in situ X-ray absorption spectroscopy.

Tirma Herranz[1], Xingyi Deng[1], Andreu Cabot[1], Jingua Guo[2] and Miquel Salmeron[1,3]*

[1]Materials Sciences Division, Lawrence Berkeley National Laboratory, [2]Advance Light Source, Lawrence Berkeley National Laboratory, [3]Materials Science and Engineering Department, University of California, Berkeley, CA 94720, USA

RECEIVED DATE

[*]To whom correspondence should be addressed. E-mail: MBSalmeron@lbl.gov

The influence of particle size in the carbon monoxide hydrogenation reaction has been studied using cobalt nanoparticles (NP) with narrow size distribution prepared by colloidal chemistry. The surfactant covering the NP after synthesis could be removed by heating to 200-270ºC in H_2. Soft X ray absorption spectroscopy was performed in a gas flow cell under reaction conditions of H_2 and CO at atmospheric pressure. Flow of pure hydrogen at 350ºC removed the protecting surfactant layer and reduced the NP from oxidized to metallic. The NP remained metallic during the methanation reaction with their surface covered by CO. The methanation turnover frequency of silica supported NP was found to decrease with diameter below 10 nm, while the reaction activation energy was found to be independent of NP size. H-D exchange experiments indicated that it is the dissociation of H_2 that is responsible for the observed decrease in activity with size.

KEYWORDS. Cobalt, nanoparticles, Fischer-Tropsch, X-ray absorption (XAS), in situ studies, soft x-ray spectroscopy, particle size dependence.

1. Introduction

Cobalt nanoparticles (NP) have found applications in data storage devices and sensors, thanks to their magnetic properties [1,2]. Cobalt is also a well known catalyst for many reactions, including growth of carbon nanotubes [3], oxidation of carbon monoxide [4], selective reduction of nitrogen oxides [5] and Fischer-Tropsch (FT) synthesis [6,7]. Its usefulness in FT synthesis is due to its low water-gas shift activity so that it is able to produce liquid hydrocarbons with high carbon efficiency [8].

To increase catalytic performance the catalyst metal dispersion should be maximized [9]. Typical cobalt catalysts are prepared from a metallic salt deposited by impregnation over an oxide support (Al_2O_3 or SiO_2), followed by several steps of drying and calcination. The precursor is a cobalt spinel (Co_3O_4), which is inactive for Fischer-Tropsch synthesis. This oxide is reduced to the active metallic cobalt phase prior to the reaction [10]. The reducibility of cobalt is a key factor in its catalytic performance. The Co_3O_4 particles are easy to reduce completely but in supported catalysts reduction is difficult when the diameter is below 6 nm [11]. If the reduction step is not complete the catalytic performance decreases [12]. The use of NP instead of precursor salts results in improved catalytic activity due to the lower interaction of the active phase with the support, as described previously [13-16].

Several papers have reported that the turnover frequency or activity per surface site decreases dramatically when the catalyst particle size reaches a critical point [13,17,18], a behaviour that is not well understood. Recently, synthesis of Co nanoparticles with diameters between 3 and 12 nm and narrow size distribution has been successfully accomplished using colloidal methods [19]. The availability of NP with such narrow size distributions makes it possible to explore size and shape effects that might be important in affecting reactivity and selectivity. These effects are masked when the size distributions of the Co particles is broad, as typically obtained when prepared by impregnation techniques.

Knowledge of the chemical state of the NP and of the species adsorbed during the FT reaction is also lacking, thus preventing a complete understanding of the catalytic process. This is due to the lack of suitable characterization techniques able to characterize the chemical and electronic structure of the catalyst during reaction. To remedy this we use X-ray absorption spectroscopy (XAS), a synchrotron-based technique for studying the electronic structure of matter. The X-rays can easily penetrate through gases at atmospheric pressure over distances of millimeters and excite electrons from core levels of atoms and molecules in the catalyst. Soft X-ray absorption edges have the important advantage of being sharp, due to the long lifetime of the core states. XAS is sensitive to details of the electronic structure, such as the valence level structure, symmetry, spin state, etc. The use of soft X-rays for the study *in situ* of cobalt catalysts was first reported by Bazin *et al.* [20,21]. In these studies, spectra of a powder Co/SiO_2 sample were obtained in the presence of hydrogen. However, the partial pressure was 10^{-4} Pa ($<10^{-6}$ torr), far from the conditions used in the industrial systems and the catalysts could not be reduced even after heating at 650ºC for 30 minutes. In the present work we used a specially designed gas flow reaction cell that made it possible to acquire XAS spectra at atmospheric pressure and at temperatures as high as 360ºC, which is similar to the temperature used in real industrial conditions. However, the pressure is still lower than the 20-30 bar used in industrial reactors.

2. Experimental section

The synthesis of the cobalt nanoparticles is described elsewhere [22]. Briefly, in an inert atmosphere a carbonyl precursor, $Co_2(CO)_8$, was decomposed in 1,2-dichlorobenzene at a temperature near its boiling point (~182ºC) [23,24]. Rapid injection of organometallic reagents in the hot solvent produces discrete and homogeneous nucleation sites. Oleic acid, $CH_3(CH_2)_7CH=CH(CH_2)_7CO_2H$, and trioctylphosphine oxide, $(CH_3(CH2)_7)_3P=O$, were used to control the growth and to provide a protective surfactant capping layer. Monodispersed Co NP with diameters between 3 and 10 nm (±0.5 nm) were prepared by adjusting the amount of oleic acid used in the synthesis. Following synthesis the samples were cleaned several times by precipitation with alcohols and re-dispersion in chloroform. The size of the NP was

determined by transmission electron microscopy (TEM) using a JEOL 2100-F 200 kV instrument. Figure 1 shows a typical TEM micrograph of 5.3 nm NP along with the measured size distribution.

The NP dispersed in chloroform were supported over high area commercial SiO_2 (Cab-O-Sil H-5 Cabot Corporation, 300 m^2/g) by wet impregnation. We choose silica because its interaction with cobalt is weak [7]. After impregnation the samples were dried at 110ºC for 16 hours. The loading was measured by inductively coupled plasma atomic emission spectroscopy, (Galbraith laboratories) and varied from 1.5 to 7 wt.%. Table 1 lists the names, loading and mass of all the catalysts used in this study. Figure 2 shows a TEM micrograph of 5.3 nm supported Co nanoparticles. As can be seen the nanoparticles have roughly spherical shapes and are well dispersed over the silica support.

Catalytic hydrogenation of CO was performed in a U-shaped quartz flow reactor using an amount of sample between 70 and 200 mg. The conditions were chosen to maximize the methane yield in the $CO+3H_2 \rightarrow CH_4 + H_2O$ reaction.

To avoid diffusion limitations, the powder samples were pelletized, crushed and sieved to obtain a pellet size of 0.25-0.30 mm [7]. The reactor was placed in an oven connected to a PID temperature controller (Watlow). The gas flow was regulated by mass flow controllers (Porter Instruments). To remove the surfactant and reduce the cobalt oxide to metal the samples were heated from room temperature to 650ºC at a heating rate of 5ºC/min in a 10% H_2/Ar atmosphere (total flow rate 50 ml/min). The CO hydrogenation reaction was subsequently measured at increasing temperatures from 200 to 270ºC at 0.1 MPa total pressure in a $3CO/10H_2/20Ar$ gas flow of 33 ml/min. The concentration of the outlet gases was monitored using selected m/z fragment peaks measured with a quadrupole mass spectrometer connected to the reactor. The reactor used for measuring the catalytic activity is equipped with a by-pass valve that allows us to first calculate the CO conversion by looking at the decrease in mass 28 (corresponding to CO). The CO conversion was also calculated using the methane production (mass 15 fragment, representing 85% of the maximum signal of methane in the spectrometer) and assuming a 100% selectivity. As we use Ar as internal standard, the calculation of the CO conversion is not affected by the the differences in gas flow or by changes in the pressure of the chamber connected to

the mass spectrometer. In all the catalysts tested the conversion values calculated using the decrease in mass 28 and mass 15 were the same within 5%.

For comparison the catalytic activity of two reference samples, a standard one and a physical mixture, was also measured. The standard sample (labelled Co/SiO_2-St) was prepared by incipient wetness impregnation [25] using $Co(NO_3)_2$ (98+%, Sigma-Aldrich) as precursor. After impregnation the sample was dried for 16 h at 110ºC and calcined in air for 2 h at 300ºC.

Another type of catalyst, in the form of a physical mixture (labelled PM) was prepared by mixing cobalt spinel (Co_3O_4), obtained from $Co(NO_3)_2$ after a thermal treatment in air (2h at 200ºC) and silicon oxide.

In situ XAS experiments were performed in the total electron yield mode using a specially designed gas flow cell at the undulator beamline 7.0.1 of the Advanced Light Source (Berkeley, USA) [26]. Details of the design, shown schematically in Figure 3, are described elsewhere [22]. The NP were deposited on a gold foil using the Langmuir-Blodgett (LB) technique [27,28]. Before the spectroscopy measurements, the samples were characterized by scanning electron microscopy (Zeiss Gemini Ultra-55) and X-ray photoelectron spectroscopy (PHI 5400).

The gold support was placed on a stainless steel holder attached to a button heater. A k-type thermocouple located under the sample was used to measure the temperature and a shielded cable spot welded to the sample holder was used for electron yield measurements. The sample and reaction chamber are located inside a UHV chamber connected to the synchrotron ring, and separated from it by a Si_3N_4 membrane window 0.5 mm^2 in area and ~100 nm thick. XAS at the Co-L and O-K edges were recorded with an energy resolution of 0.3 eV. A cobalt foil was used for energy calibration. The use of total electron yield to record XAS makes the method surface sensitive (to a depth in the nm range), as compared with the bulk sensitive fluorescence yield detection mode.

3. Results and discussion

3.1. Catalytic activity of SiO_2 supported catalysts

Treatment of the samples in 10% H_2 in He prior to the catalytic reaction yielded various products as the temperature increased, as shown in Figure 4. First, between 100ºC and 200ºC carbon dioxide, water and methane evolved due to decomposition of the surfactant. Between 300 and 450ºC a broad water peak appears that corresponds to the reduction of CoO to metallic cobalt [29]. At 550-650ºC methane evolution was observed, which we assign to the hydrogenation of carbonaceous species on the surface of the catalyst. The area of the peaks, normalized by the total amount of cobalt in the samples indicated that the amount of methane and carbon dioxide was larger for the smaller particles, as expected from the fact that the smaller particles display more surface area. This point was also confirmed by thermogravimetric analysis.

After reduction the catalytic activity for CO hydrogenation was measured at ambient pressure and different temperatures in the 200-270ºC range. In addition to methane, mass fragments corresponding to products such as ethylene, ethane, propylene and propane, were also monitored. Specifically the fragments corresponding to m/z = 27, 29 and 41 were monitored using QMS during all reaction experiments. The peak at m/z = 27 corresponds to fragmentation of ethylene and ethene (60 and 70% of the maximum signal in mass spectrometry) and the fragment at m/z = 41 corresponds to the maximun signal in the fragmentation spectrum of propene. As the products of the Fisher-Tropsch synthesis in the absence of promoters follow the Anderson-Schulz-Flory distribution, the main products (by weight) will correspond with the C1-C3 fraction in the reaction conditions studied (low alpha, relatively high temperature and high hydrogen to carbon monoxide ratio). We did not observe any increment of the cited fragments during reaction, implying that hydrocarbons above C1 were produced in concentrations below the detection limit of our QMS. In the samples prepared using NP the production of methane was stable at every temperature studied with no decrease in activity over time. However, the sample prepared by impregnation (Co/SiO_2-St) showed a strong deactivation at higher temperatures (over 250ºC), a behaviour attributed to sintering of the particles [12] or to reactions with the support that produce cobalt silicates [30].

Figure 5a shows the turnover frequency (number of CO molecules converted per exposed Co atom per second) measured at 240ºC as a function of NP diameter. The turnover frequency increased with diameter, in agreement with previous reports, reaching a stable value for diameters larger than 10 nm [17]. The value of 25 nm in the graph corresponds to samples prepared by physical mixture, which show the highest turnover, although the activity per gram of catalyst was very low. When the activity is expressed as number of CO molecules converted per gram of cobalt, it is larger for the smaller sizes, because of the higher fraction of exposed cobalt atoms. The activation energy (kcal/mol) calculated from Arrhenius plots of activity versus 1/T for each particle size is displayed in Figure 5b. The values are very similar for all diameters, indicating that the rate determining step is the same for all the particle sizes.

3.2 Preparation of 2-D model catalysts

A single layer of nanoparticles was deposited over a conductive flat gold substrate using the LB technique. The particles were first washed to remove the excess of surfactant. Because of its low vapour pressure the original dichlorobenzene solvent was substituted by chloroform for LB preparation. A few droplets of the NP dispersed in chloroform were spread over a trough filled with distilled water at room temperature. The surface pressure of the film was controlled with two Teflon barriers that compress it. Several samples were prepared at increasing surface pressures. As reported before [31] the nanoparticles are distributed homogeneously over the support even at low pressure, with a loading that can be increased with surface pressure. Although the as-prepared nanoparticles are in the metallic state [19] and show a sharp size distribution (Figure 1), the cleaning process and the transfer to the gold support caused oxidation of the particles to CoO [32,33], as confirmed by electron diffraction and XPS. Figure 6 shows SEM pictures of two different samples prepared in this way. The SEM pictures were acquired with low electron energy (1 kV) to minimize beam damage (the particles are still covered by surfactant). To reduce contamination, after preparation the samples were kept in a dry box with N_2 flowing.

3.3 In situ XAS experiments

Model catalysts consisting of Co nanoparticles supported on a Au foil were prepared using the Langmuir-Blodgett technique and studied *in situ* (i.e., in reaction conditions of gas pressure and

temperature) in the XAS cell. In Figure 7 we show the evolution of $2p_{3/2}$ and $2p_{1/2}$ core levels of selected Co NP during reduction of the samples at increasing temperatures in a 40 ml/min stream of pure H_2 at 0.1 Mpa. For all particle sizes the spectra at room temperature correspond to CoO [20], which contains Co^{2+} ions octahedrically coordinated with oxygen anions. The presence of this cobalt oxide is evidenced by the extra features at 776.5 and 780 eV. During the heating treatment in hydrogen from 250ºC to 330ºC, the features in the X-ray absorption spectra changed to those of the metallic state characterized by two asymmetric absorption white lines at 778 and 794 eV as it was described by Morales *et al.* [34]. In this earlier work the influence of promoters and the support on the Co reducibility was studied using *in-situ* XAS with a hydrogen pressure of 2 mbar. However, the influence of the particle size was not analyzed as the samples were prepared by homogeneous deposition precipitation from a Co nitrate precursor solution. Unlike the case of cobalt supported on oxide powders [7], our experiments revealed that the smaller nanoparticles were easier to reduce than the larger ones. The 3 nm sample was completely reduced after a flash heating at 330ºC. When the size increased to 4.2 nm is was necessary to heat for 2 minutes at 330ºC to reach complete reduction. For the 10 nm nanoparticles the reduction was not completed until after 8 minutes.

After reduction, the H_2 atmosphere was switched to pure carbon monoxide and the changes in the electronic structure of the nanoparticles were followed both at room temperature and after heating. As shown in Figure 8 the Co L-edge spectra of the cobalt foil and 3 nm NP did not change after flowing CO at room temperature or heating in CO or H_2+CO mixtures. Similar results were obtained with other NP sizes. To obtain spectra of the O K-edge the CO gas flow was stopped and the line purged with hydrogen to avoid x-ray absorption by the gas phase. As expected, the reduced samples show no features in the O K-edge spectra (Figure 9a). After exposing to the CO gas flow at room temperature, a large absorption peak at 534.2 eV appeared. This peak was still present after purging the line with hydrogen, as shown in Figure 9a for the 4.2 nm NP sample. We ascribe this peak to CO adsorbed on the cobalt NP, because in the conditions studied (room temperature and ambient pressure) carbon monoxide did not react with the cobalt surface [35]. However, when the sample was heated in a flowing hydrogen

atmosphere at 240ºC for 5 minutes the area of the peak decreased substantially due to the reaction with the flowing gas to form methane. Heating the sample for 10 minutes removed the peak completely. If the same heating treatment was performed in a flowing He atmosphere, the CO-related peak in the O K-edge at 534.2 eV decreased due to partial desorption, but was still present. It was necessary to pump the line to completely remove it. The experiment was also performed in batch mode (Figure 9b). After flowing pure CO, the cell was filled with hydrogen and then the inlet and outlet valves were closed. In this case, after heating, the 534.2 eV peak decreased although much more slowly than in flowing conditions. At the same time new features appeared at 536 and 537.2 eV, which we assign to water adsorbed on the Co surface [36]. Water is a by-product of the methanation reaction, with one molecule formed for every methane molecule. In all cases, irrespective of the particle diameter the electronic structure of the cobalt L-edge did not change during reaction.

These results show that the active phase of Co catalysts in Fischer-Tropsch synthesis is the metallic state and that it remains unchanged during the reaction. Some authors have reported oxidation of the cobalt catalysts due to the water vapour. There are indeed predictions based on theoretical calculations that support these models [37]. However, in Co/SiO_2 NP catalysts of 4-5 nm, oxidation was not observed until very high temperatures (more than 400ºC), even with a H_2/H_2O ratio of 1 [38]. This is in agreement with our XAS results, which did not show any peak assigned to cobalt oxide in the O K-edge region, and where the Co L-edge peak structure was always that of Co in the metallic state. To further confirm this result we performed another experiment treating the reduced cobalt samples with H_2/H_2O (1:1) and H_2O/He (P_{H2O}= 23 torr) in a temperature range of 25-250ºC. After exposing the reduced cobalt nanoparticles to water vapor, the Co L-edge showed none of the features characteristic of the oxide (data not shown).

3.4. Characterization of samples after reaction

After testing the catalytic activity of the Co/SiO_2 powder samples, the temperature was lowered to 25ºC and the gas flow was switched to H_2/Ar to perform a thermal treatment (TPD-H_2) to characterize the possible carbonaceous species adsorbed on the surface of the catalysts. Figure 10 shows the

evolution of the H_2O, CO, CO_2 and CH_4 signals with temperature for the 10 nm Co/SiO_2 NP catalyst. As can be seen in the graph, there is no trace of desorbed products in the temperature range studied (50-650ºC), indicating that no detectable amount of carbonaceous species were deposited on the catalyst during the CO hydrogenation.

Figure 11 shows selected TEM pictures obtained from used powder samples of 3 nm (top), physical mixture (middle) and the standard sample (bottom). The physical mixture displays large cobalt particles of irregular shape whose electron diffraction patterns corresponds to metallic cobalt and CoO. The standard sample shows a bimodal distribution of particle sizes, most of the cobalt being present as nanoparticles of 5-6 nm but large clusters are also present. In contrast, on the sample prepared using NP of 3 nm diameter, the cobalt remains spread over the support with no signs of agglomeration.

Figure 12 shows a high resolution SEM micrograph of the 10 nm 2D model catalysts after reduction in H_2 and treatment with H_2 and CO at high temperature. The NP retained their morphology and size even after the high temperature treatment.

3.5. H-D exchange experiments

The differences in catalytic activity as a function of particle diameter cannot be attributed to oxidation of the catalysts during reaction, as shown by the *in situ* XAS results. The lack of deactivation with time of the NP catalysts is also consistent with these observations. Deactivation by carbon deposition can also be ruled out, as demonstrated by the fact that temperature-programmed treatment in hydrogen of all the samples after reaction did not produce carbon-containing products. Finally, sintering of the NP can be discarded as shown by the SEM and TEM micrographs of the used samples that show no agglomeration of the NP.

It is clear that in any case the dissociative adsorption of hydrogen molecules plays a major role in the reaction mechanism. Although it is believed that at saturation hydrogen chemisorption involves one hydrogen atom per cobalt surface site [39], the dissociative step might require a particular geometry of contiguous empty Co sites with a minimum of two or more sites. Indeed it has been shown that on Pd, Pt and Ru hydrogen dissociation requires at least three adjacent sites [40-42], so that the dissociative

probability p will not follow a simple Langmuir law $p \propto (1-x)^n$ function, with n> 2 or even a more complicated dependence depending on site geometry. In this model, hydrogenation of CO would require three or more adjacent sites to dissociate hydrogen and at least one more for CO adsorption, as in the H-assisted CO dissociation mechanism suggested by King et al. [43]. The probability of finding these larger ensemble sites should decrease rapidly for the smaller particles and explain at least qualitatively the drop in the turnover frequency with lower particle diameters.

To test this model we performed H-D exchange experiments on selected samples of reduced cobalt NP supported on SiO_2 powder. After reducing the samples with hydrogen at 500ºC, they were cooled down to room temperature and then exposed to a flowing mixture of H_2/D_2/Ar (20:20:60, 50 ml/min). The temperature was then increased slowly (1ºC/min) and the concentration of HD was measured at 10 ºC intervals in the 40-90ºC range. The signals of hydrogen (m/z = 2), deuterium (m/z = 4) and HD (m/z = 3) were monitored on-line using mass spectrometry. Figure 13 shows the turnover frequency for HD production as a function of temperature and particle diameter. The specific activity for HD production increases with temperature as expected, but more significant, the HD turnover frequency decreases with particle size. The behaviour with temperature is also different in the cobalt nanoparticles with diameters below 10 nm. HD production in those samples reaches a steady state at temperatures below 100ºC. These results demonstrate that the hydrogen dissociation is structure sensitive for particles with size below 10 nm. Although at present we do not have a detailed model to explain the evolution of the H-D exchange TOF with size and temperature and that more experiments are needed for a full understanding, we believe the observations point strongly to the adsorption and dissociation of H_2 as mechanism responsible for the particle size dependence of the methanation reaction. We further propose that the limiting factor in H_2 adsorption is the availability of large ensembles of Co atoms on the surface of the nanoparticles.

4. Conclusions

Monodispersed cobalt nanoparticles prepared by colloidal chemistry methods have been used to study the structure sensitivity of the CO hydrogenation reaction. Powder samples supported on silicon oxide

and on gold have been prepared using Co nanoparticles from the same batch. The chemical state of the nanoparticles and the changes occurring during reaction were investigated using in-situ soft X-ray absorption spectroscopy at atmospheric pressure and temperature up to 330ºC. We have shown that the surfactant ligands can be readily removed by heating in H_2 and that the nanoparticles are in the metallic state and covered with CO during methanation. Our electron microscopy studies have shown that the particles do not sinter as a result of the heating treatments to remove surfactants, or during the reaction.

We have also shown that the methanation activity decreases with particle size below 10 nm and that this reduction is not due to carbon deposition, sintering or oxidation by water vapor. Notably we have shown that the activation energy for methanation remains constant with particle size, indicating that the rate limiting step is unchanged. Hydrogen-deuterium exchange experiments show that the specific activity in the HD production decreases also when the particle size decreases below 10 nm and demonstrates that the dissociative adsorption of H_2 is the important factor responsible for the size effect. We interpret our results with a model where large ensembles (more than four sites) are required for the hydrogen molecule dissociative adsorption, a key starting step in any model mechanism of CO methanation.

ACKNOWLEDGMENT. We thank Prof. Paul Alivisatos for his support in the synthesis of nanoparticles and careful reading of this paper. This work was supported by the Director, Office of Science, Office of Basic Energy Sciences, Chemical Sciences, Geosciences, and Biosciences Division, under the Department of Energy Contract No. DE-AC02-05CH11231. Synthesis and characterization of the nanoparticles was performed in the Molecular Foundry and at the Advanced Light Source. T.H. acknowledges also the financial support from the Ramon Areces Foundation from Spain.

REFERENCES

1. Qiang, Y., *J. Phys. Rev. B*, **2002**, *66*, 064404.

2. Petit, C., *J. Phys. Chem. B.*, **2003**, *107*, 10333.

3. Terrado, E., *Mater. Sci. Eng. C*, **2006**, *26*, 1185.

4. Yang, W.H., Kim, M.H., Ham, S.H., *Catal. Today*, 2007, *123*, 94.

5. Armor, J.N., *Catal. Today*, **1995**, *26*, 147.

6. Dry, M.E., *Catalysis Sciences and Technologie*, J.R. Anderson and M. Boudart Editors, Vol. 1 p. 159. Springer Verlag, Berlin, 1981.

7. Khodakov, A.Y., Chu, W., Fongarland, P., *Chem. Rev.*, **2007**, *107* 1692.

8. Jacobs, G., Das, T., Zhang, Y., Li, J., Racoillet, G., Davis, B.H., *Appl. Catal. A: Gen.*, **2002**, *233*, 263.

9. Soled, S.L., Iglesia, E., Fiato, R.A., Baumgartner, J.E., Vroman, H., Miseo, S., *Top. Catal.*, **2003**, *26*, 101.

10. Iglesia, E., *Appl. Cat. A: Gen.*, **1997**, *161*, 59.

11. Khodakov A.Y., *J. Catal.*, **1997**, *68*, 16.

12. Niemelä, M.K., Backman, L., Krause, A.O.I., Vaara, T., *Appl. Catal. A: Gen.*, **1997**, *156*, 319.

13. Martinez, A., Prieto, G., *J. Catal.*, **2007**, *245*, 470.

14. Rioux, R.M., Song, H., Hoefelmeyer, J. D., Yang, P., Somorjai, G. A., *J. Phys. Chem. B*, **2005**, *109*, 2192.

15. Zheng, N., Stucky, G.D., *J. Am. Chem. Soc.*, **2006**, *128*, 14278.

16. Herranz, T., Rojas, S., Pérez-Alonso, F.J., Ojeda, M., Terreros, P., Fierro, J.L.G., *Appl. Catal. A:Gen.*, **2006**, *308*, 19.

17. Bezemer, G.L., Bitter, J.H., Kuipers, H.P.C.E., Oosterbeek, H., Holewijn, J.E., Xu, X., Kapteijn, F., van Dillen, A.J., de Jong, K.P., *J. Am. Chem. Soc.*, **2006**, *128*, 3956.

18. Yu, Z., Borg, O., Chen, D., Enger, B.C., Froseth, V., Rytter, E., Wigum, H., Holmen, A., *Catal. Let.*, **2006**, *109*, 43.

19. Puntes, V.F., Krishnan, K.M., Alivisatos, A.P., *Science*, **2001**, *291*, 2115.

20. Bazin, D., Kovacs, I., Guczi, L., Parents, P., Laffon, C., de Groot, F., Ducreaux, O., Lynch, J., *J. Catal.*, **2000**, *189*, 456.

21. Bazin, D., Guczi, L., *Appl. Catal. A:Gen.*, **2001**, *213*, 162.

22. Liu, H., Guo, J., Yin, Y., Augustsson, A., Dong, C., Nordgren, J., Chang, C., Alivisatos, A.P., Thornton, G., Ogletree, D.F., Requejo, F.G., de Groot, F., Salmeron, M., *Nano Lett.*, **2007**, *7*, 1919.

23. Puntes, V.F., Gorostiza, P., Aruguete, D.M., Bastus, N.G., Alivisatos, A.P., *Nat. Mater.*, **2004**, *3*, 263.

24. Puntes, V.F., Krishnan, K.M., Alivisatos, A.P., *Appl. Phys. Lett.*, **2001**, *78*, 2187.

25. Ojeda, M., Pérez-Alonso, F.J., Terreros, P., Rojas, S., Herranz, T., López Granados, M., Fierro, J.L.G., *Langmuir*, **2006**, *22*, 3131.

26. Nordgren, J., Guo, J.H., *J. Electron. Spectrosc. Relat. Phenom.*, **2001**, *110-111*, 1.

27. Heath, J.R., Knobler, C.M., Leff, D.V., *J. Phys. Chem. B*, **1997**, *101*, 189.

28. Rioux, R.M., Song, H., Grass, M., Habas, S., Niesz, K., Hoefelmeyer, J.D., Yang, P., Somorjai, G.A., *Top. Catal.*, **2006**, *39*, 167.

29. Jacobs, G., Ji, Y., Davis, B.H., Cronauer, D., Kropf, A.J., Marshall, C.L., *Appl. Cat. A: Gen.*, **2007** *333*, 177 .

30. Puskasa, I., Fleischa, T.H., Fulla, P.R., Kaduka, J.A., Marshallb C.L., Meyersa, B.L., *Appl. Catal. A:Gen.*, **2006**, *311*, 146.

31. Song, H., Kim, F., Connor, S., Somorjai, G.A., Yang, P., *J. Phys. Chem. B*, **2005**, *109*, 188.

32. Yang, H.T., Shen, C.M., Wang, Y.G., Su, Y.K., Yang, T.Z., Gao, H.J., *Nanotechnology*, **2004**, *15*, 70.

33. Bao, Y.P., Beerman, M., Pakhomov, A.B., Krishnan, K.M., *J. Phys. Chem. B*, **2005**, *109*, 7220.

34. Morales, F., de Groot, F.M.F., Glatzel, P., Kleimenov, E., Bluhm, H., Hävecker, M., Knop-Gericke, A., Weckhuysen, B. M., *J. Phys. Chem. B*, **2004**, *108* 16201.

35. Beitel, G.A., Laskov, A., Oosterbeek, H., Kuipers, E.W., *J. Phys. Chem.*, **1996**, *100*, 12494.

36. Stöhr, J., NEXAFS spectroscopy. Sping Series in Surface Sciences (2nd print) 2003.

37. van Steen, E., Clayes, M., Dry, M.E., van der Loosdrecht, J., Vilkoen, E.L., Visagie, J.L., *J. Phys. Chem. B*, **2005**, *109*, 3575.

38. Saib, A.M., Borgna, A., van de Loosdrecht, J., van Berge, P.J., Niemantsverdriet, J.M., *J. Phys. Chem. B*, **2006**, *110*, 8657.

39. Reuel, R.C., Bartholomew, C.H,, *J. Catal.*, **1984**, *85*, 63.

40. Mitsui T., Rose M.K., Fomin, E., Ogletree D.F., Salmeron, M., *Nature*, **2003**, *422*, 705.

41. Montano, M., Bratlie, K., Salmeron, M., Somorjai, G.A., *J. Am. Chem. Soc.* **2006**, *128*, 13229.

42. Rose, F., Tartakhanov, M., Fomin, E., Salmeron. M., *J. Phys. Chem. C.*, **2007**, *111*, 19052.

43. Inderwildi, O.R., Jenking, S.J., King, D.A., *J. Phys. Chem. C*, **2008**, *112*, 1305.

TABLE OF CONTENTS

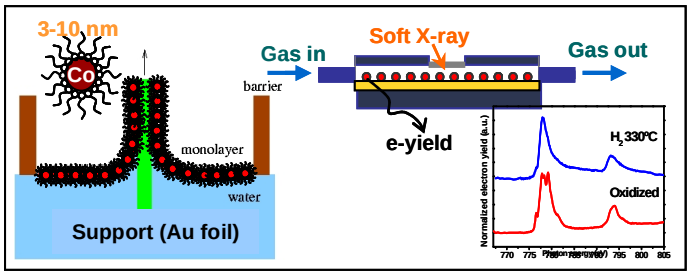

Table 1. Catalysts used in this study. They include Co nanoparticles on SiO_2 powder, as a function of diameter (in nm), a standard catalyst prepared by impregnation (St), and a physical mixture (PM).

Name	*Particle diameter (nm)*	*Loading (% wt.)*	*Mass of catalyst used (mg)*
CoSiO2-3	3.0	7.0	70
CoSiO2-4.2	4.2	3.3	74
CoSiO2-4.6	4.6	2.5	180
CoSiO2-5.3	5.3	2.9	70
CoSiO2-10	10.0	1.3	230
CoSiO2-St	8	12.0	100
CoSiO2-PM	25	3.7	200

FIGURES.

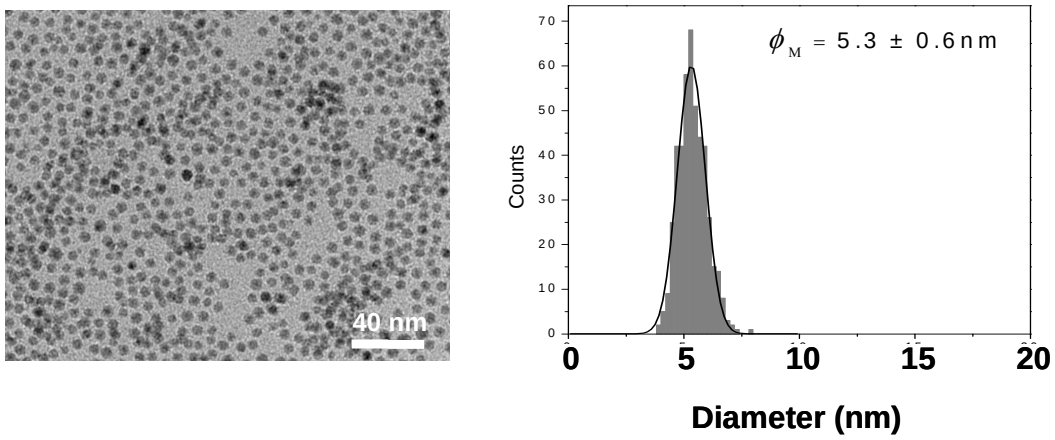

Figure 1. Left: Transmission Electron Micrograph (top) of 5.3 nm cobalt particles. Right: plot of the particle size distribution.

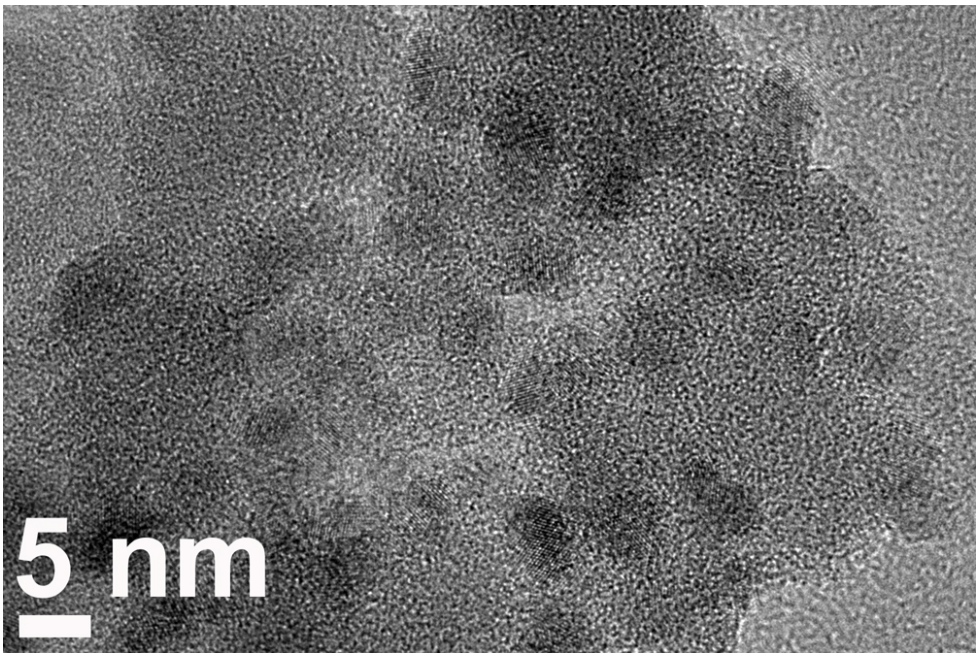

Figure 2. Transmission Electron Micrograph of the 5.3 nm Co particles supported on SiO_2 powder

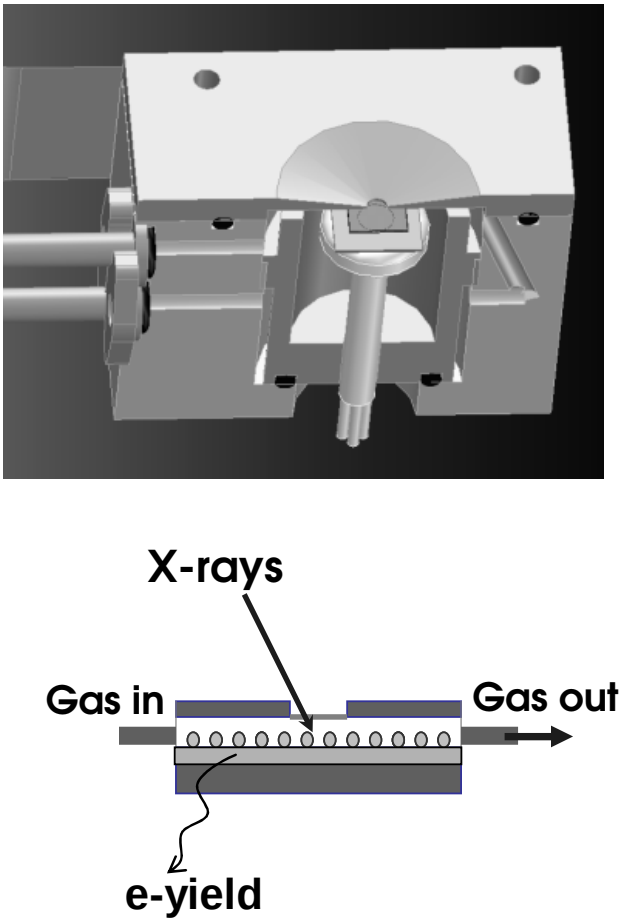

Figure 3. Drawing and schematic diagram of the gas-flow cell used for in-situ X-ray absorption measurements.

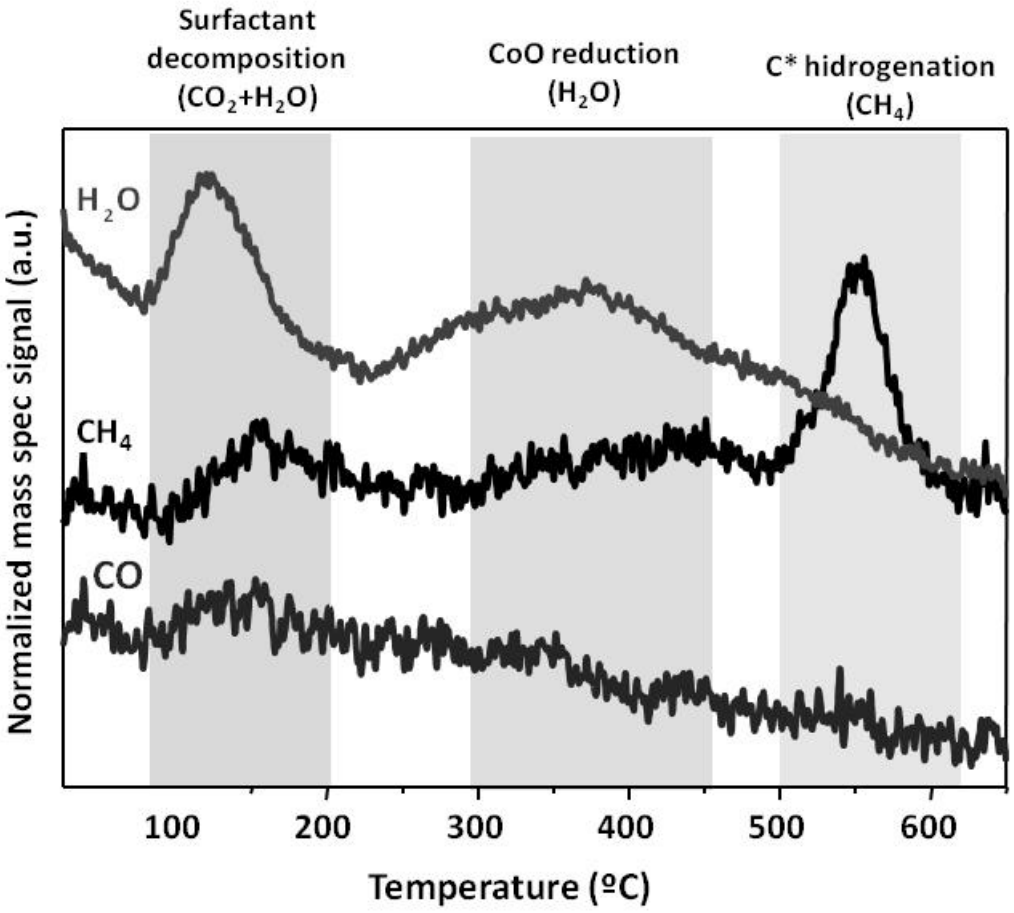

Figure 4. Products evolved from the the 10 nm Co/SiO_2 samples during temperature-programmed treatment in a H_2/Ar stream.

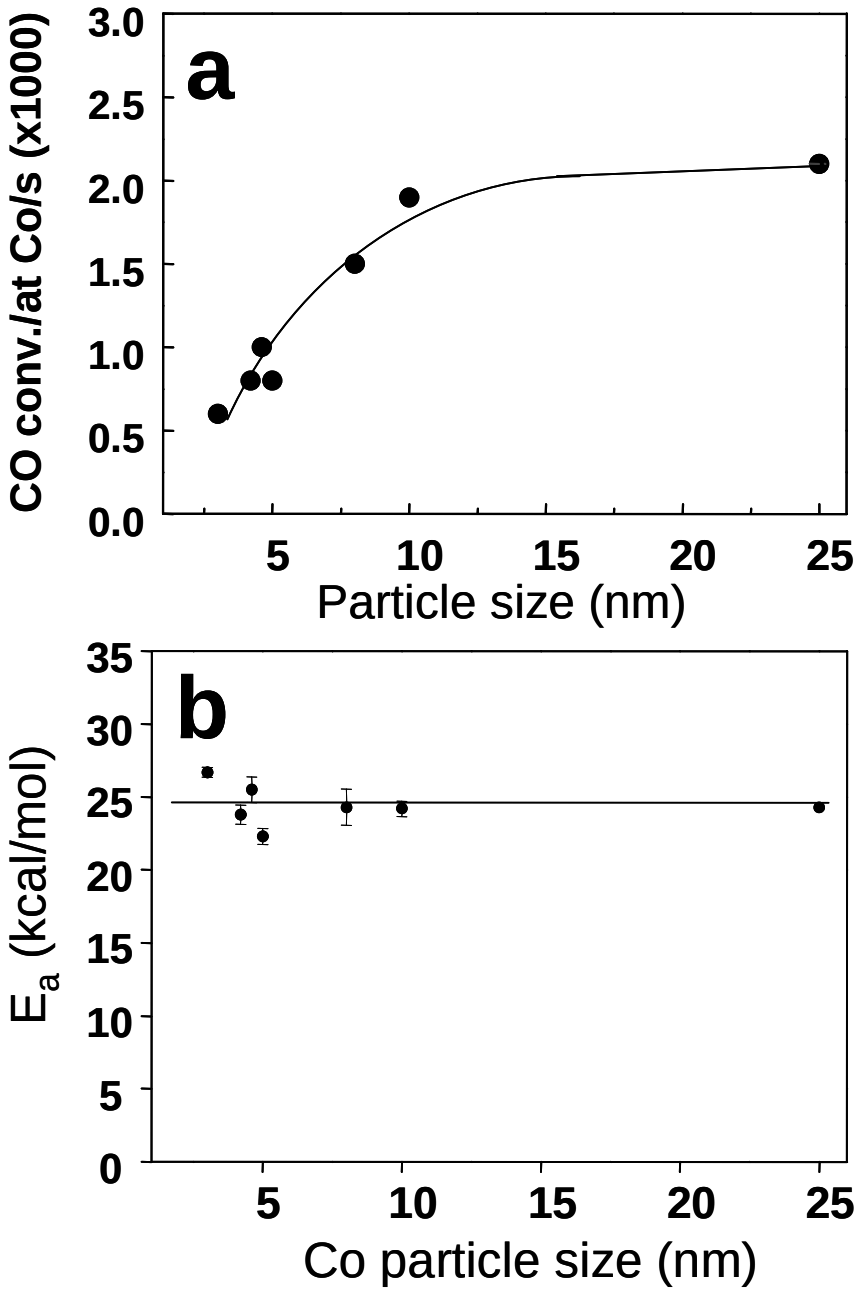

Figure 5. Catalytic activity for CO hydrogenation in a 3 CO/10H_2/20 Ar gas flow mixture at a pressure of 0.1 MPa. a) Turnover frequency at 240ºC (the line is a visual guide only), and b) activation energy, as a function of particle diameter.

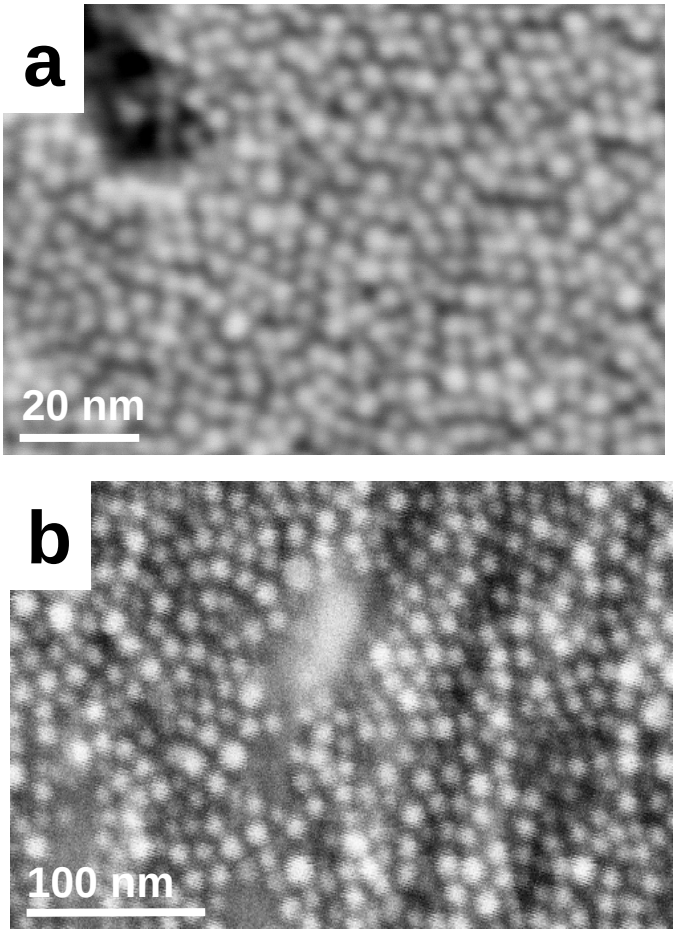

Figure 6. Scanning Electron Micrographs of Cobalt nanoparticles (NP) transferred onto Au foils using the Langmuir-Blodgett techniques. a) 3 nm NP; b) 10 nm NP.

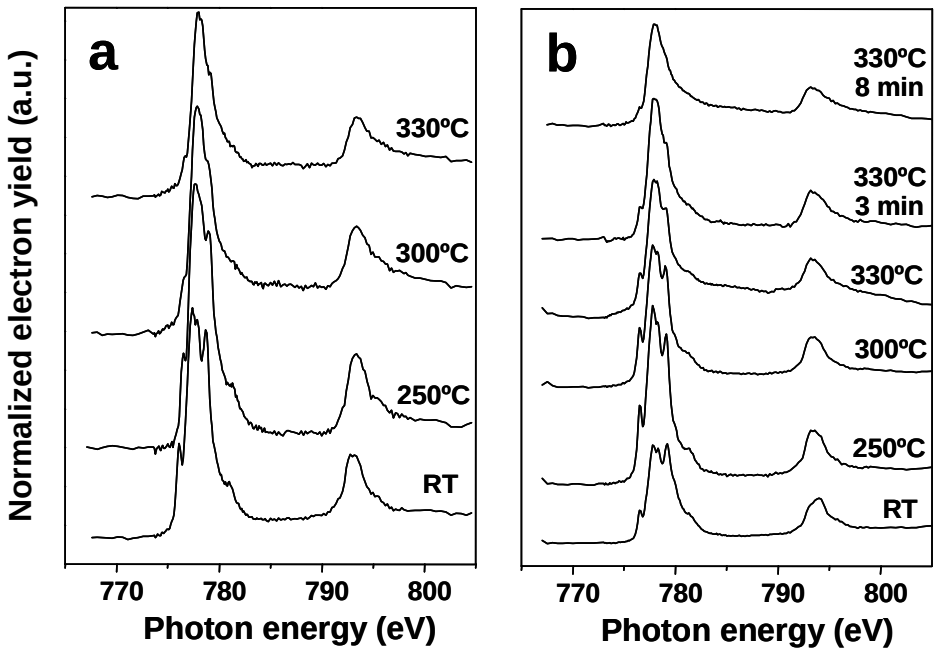

Figure 7. Co L-edge spectra of cobalt nanoparticles deposited over Au foils acquired in-situ during reduction in pure hydrogen. Particle diameters are: a) 3nm; b) 10 nm.

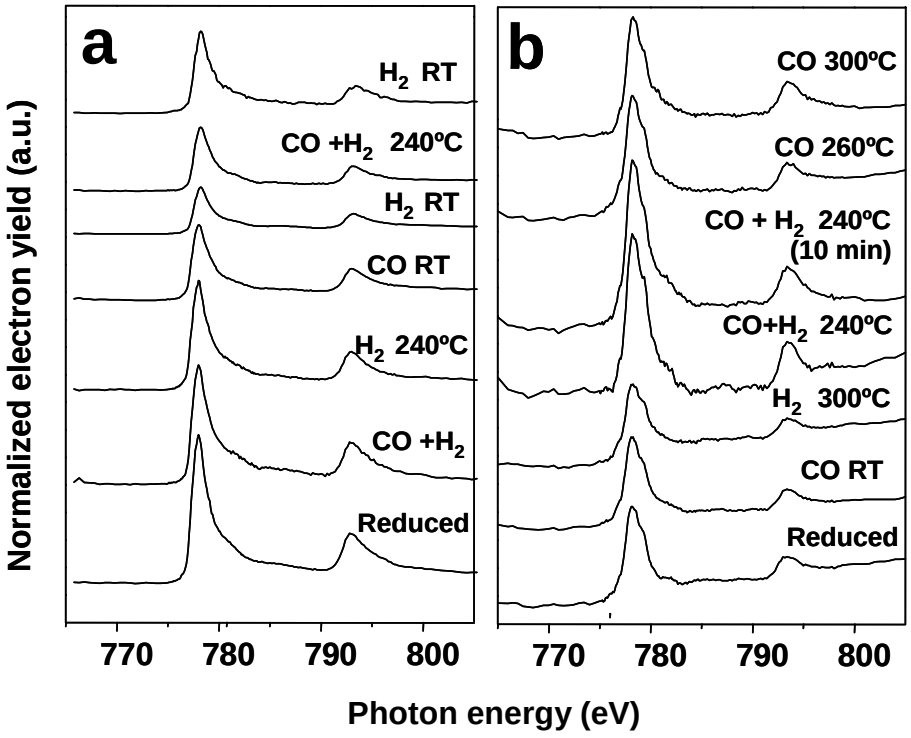

Figure 8. XAS of the Co L-edge for a cobalt foil (a), 3 nm Co NP (b), and 4.2 nm (c) Co NP during treatment with carbon monoxide (CO) and syngas (H2+CO) at different temperatures.

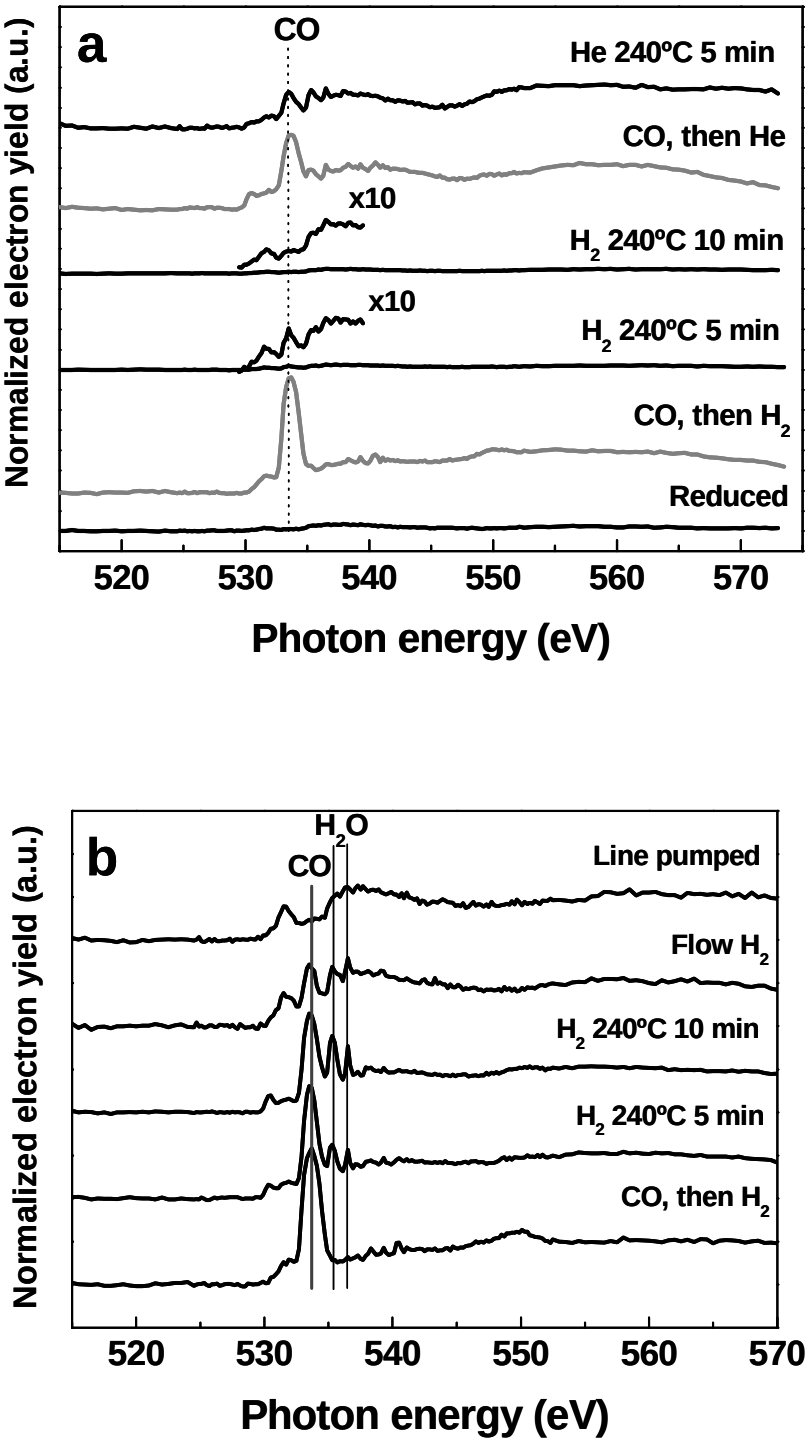

Figure 9. O K-edge of 4.2 nm cobalt NP after exposure to CO and after heating in H_2 and He. First, CO was flown over the sample and then the sample was heated at 240ºC in either in H_2 or He in flow mode (a), or in H_2 in batch mode (b).

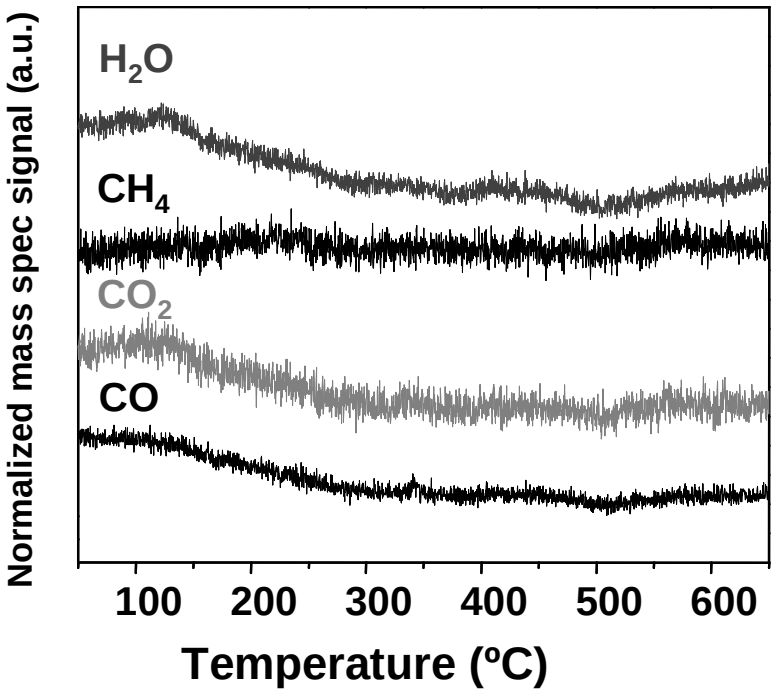

Figure 10. Products evolved during temperature programmed treatment in a H_2/Ar stream of 10 nm Co/SiO_2 sample. The samples had been used in the catalytic CO hydrogenatation reaction.

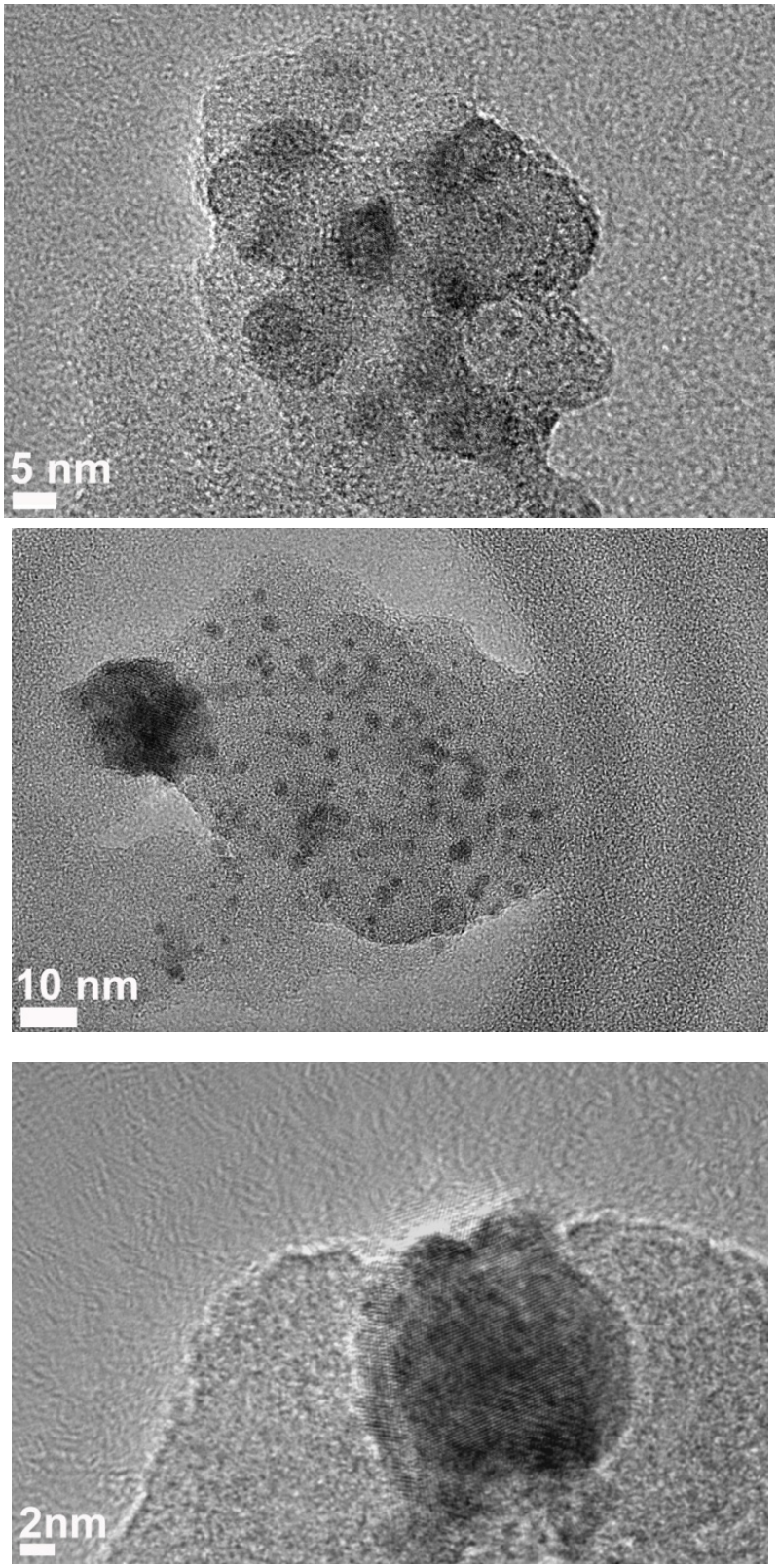

Figure 11. Transmission Electron Micrographs of Co/SiO_2 catalysts after reaction. Top: 3 nm NP; Middle: Standard sample; Bottom: Physical mixture sample.

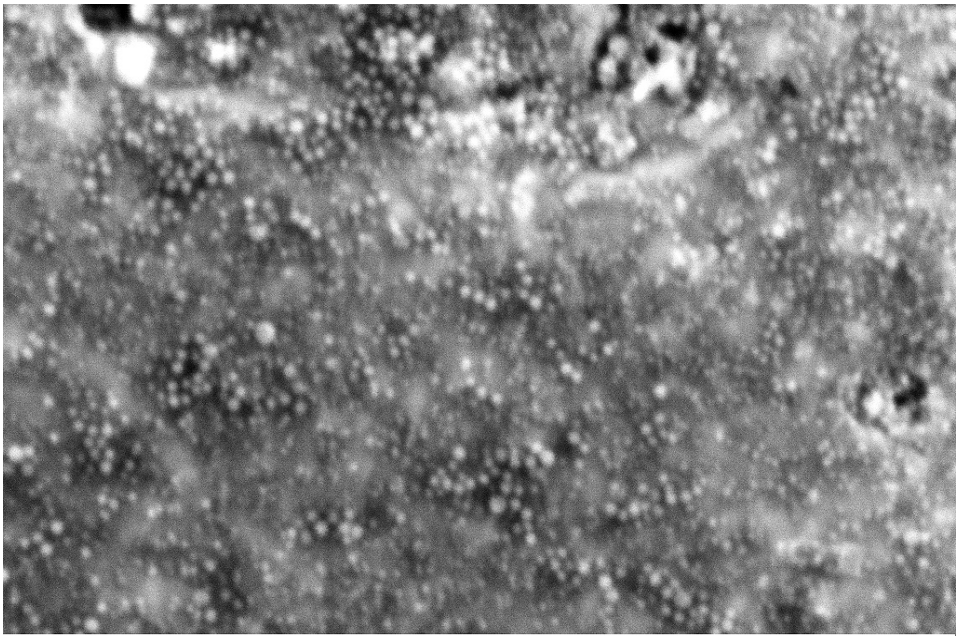

Figure 12. Scanning Electron Micrograph of 10 nm cobalt NP deposited on a Au foil after reduction in hydrogen (330-350ºC) and treatment in CO and CO+H_2 mixtures.

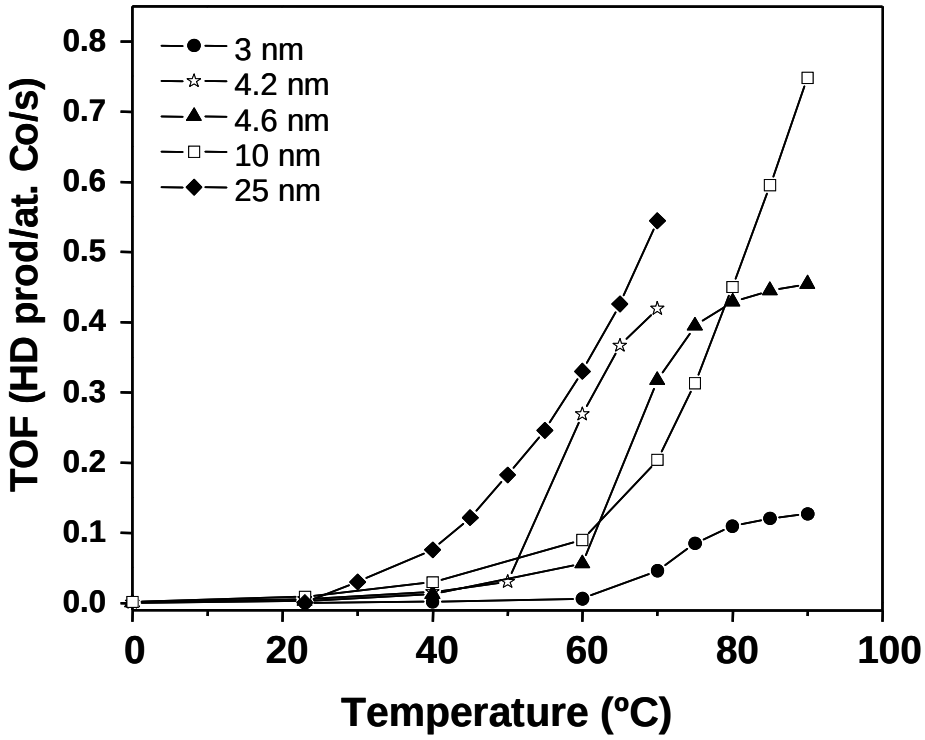

Figure 13. HD production per exposed cobalt atom as a function functions of temperature for various particle diameters.

TABLE OF CONTENTS